

Synthesis and characterization of Nd³⁺ doped SrF₂ nanoparticles prepared by precipitation method



Zhiwei Zhou^a, Weiwei Li^a, Jinghong Song^b, Guoqiang Yi^a, Bingchu Mei^{a,*}, Liangbi Su^c

^a State Key Laboratory of Advanced Technology for Materials Synthesis and Processing, Wuhan University of Technology, Wuhan 430070, China

^b Center of Materials Research and Analysis, Wuhan University of Technology, Wuhan 430070, China

^c Shanghai Institute of Ceramics, Chinese Academy of Sciences, Shanghai 200050, China

ARTICLE INFO

Keywords:

Nd³⁺ doped SrF₂ nanoparticles
Precipitation method
Transparent ceramic

ABSTRACT

The SrF₂ nanoparticles activated by Nd³⁺ were synthesized via precipitation method. The samples were characterized by X-Ray diffraction (XRD), field-emission scanning electron microscope (FESEM), energy dispersive X-ray spectrometer (EDS), high-resolution transmission electron microscopy (HRTEM) and optical transmission spectrum. The FESEM results showed that reactant concentration played significant role in the morphology and size of final SrF₂ particles. i.e., slab-like shape with about 400 × 200 × 100 nm in size SrF₂ grains were synthesized at 0.1 M reactant concentration. While a size of about 15–30 nm and near-spherical morphology particles could be obtained at 0.5–1.0 M. Due to higher probability of particles collision, the situation changes to cone-like grains with mean size of about 500 nm at 1.5 M. Observed lattice distortion from HRTEM measurement indicates successful introduction of Nd³⁺ into the SrF₂ matrix. The as-prepared Nd:SrF₂ nanopowder can be fabricated to transparent ceramic with a transmittance of about 80% at 1060 nm under vacuum hot pressed sintering at 800 °C for 2 h, indicating good sinterability of the nanopowders.

1. Introduction

Lanthanide-based luminescent inorganic nanomaterials attract growing interests during the past few years owing to their wide applications in solid state lasers [1,2], biological labeling [3], flat panel displays and thin disk lasers etc [4,5]. Considering the chemical composition, size and morphology of nanomaterials are fundamentally related to their chemical and physical properties [6–8], great endeavor aiming to obtain nano-scale particles with improved microstructure has been devoted to investigating the synthetic approaches of these materials and vast progresses have been achieved. Li and co-workers [9] reported the synthesis of monodispersed CeF₃ and NaCeF₄ nanocrystals by using liquid-solid-solution method. Fatima and co-workers [10] obtained nano-sized tetragonal scheelite-like NaGd_{1-x}Yb_x(WO₄)₂ particles via a mild hydrothermal approach, etc [11–13]. However, most of these methods usually require strict reaction conditions such as catalysts, expensive and toxic templates or surfactants, relative high temperature, costly steel autoclaves and a number of complicated procedures. As a solution, precipitation method attracts considerable attention, for it is a relatively simple way to synthesize nanopowders with composition homogeneity, good crystallinity, low react temperature as well as high productivity, and has been widely used to obtain

both transparent ceramic precursor powders and phosphors such as YAG [14], CaF₂ [15], (Y_{1-x}Gd_x)₂O₃ [16,17], Ca₂Sb₂O₇ [18].

Alkaline-earth fluorides based lasers, such as CaF₂, SrF₂, are served as promising substitution of YAG for several reasons: (i) High solubility for trivalent lanthanide ions substituting for divalent alkaline earth ions [19]. (ii) Large band gaps (above 10 eV) make them transparency in a very large frequency region (0.15–10 μm) [20]. (iii) Low phonon energy (~ 350 cm⁻¹) [21] and high thermal conductivity (8.7–9.7 W m⁻¹ K⁻¹), which are important to high power laser emitting. When doped with Nd³⁺, an attractive luminescent ion for high power laser, it is reported that the near-infrared (NIR) laser output with high power and high slope efficiency were obtained in both single crystals and polycrystalline laser ceramics [2,22,23]. Generally, compared to CaF₂, the SrF₂ host provides for a larger tolerance of Nd³⁺ dopant without the occurrence of detrimental clustering, and in addition has a remarkably long emission lifetime [24], thereby permitting the efficient extraction of energy from Nd:SrF₂ amplifiers. In spite of widely reports on Ln³⁺ doped CaF₂ [25–27], however, to our best knowledge, there have been few literatures available on systematic studies in producing Nd³⁺ doped SrF₂ via precipitation process.

Herein, we reported the preparation of SrF₂ nanopowders activated by Nd³⁺ via precipitation method. To obtain nano-sized particles, the

* Correspondence to: 122 Luoshi Road, Wuhan, Hubei, China.
E-mail address: bcmeilab@163.com (B. Mei).

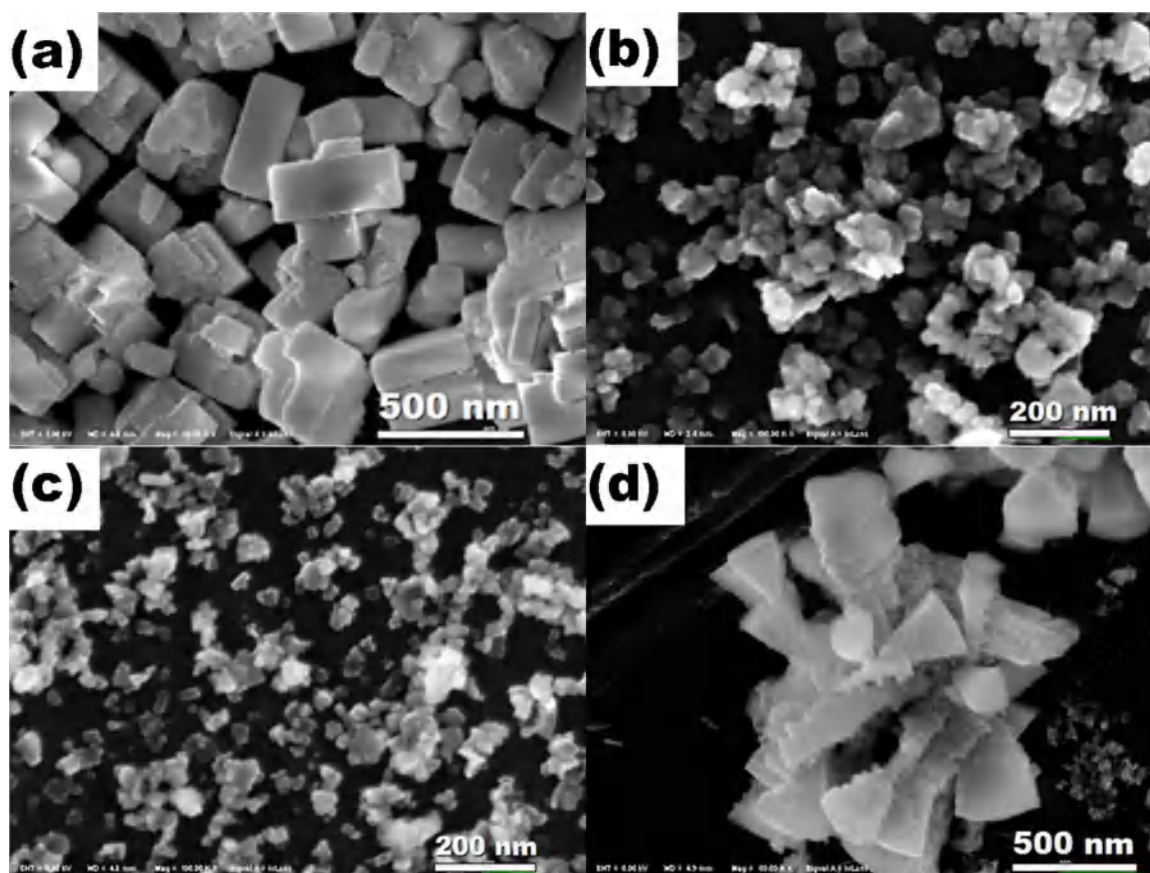


Fig. 1. FESEM images of undoped SrF_2 particles with different reactant concentration. (a) 0.1 M; (b) 0.5 M; (c) 1.0 M; (d) 1.5 M.

influence of starting reagent molarity on final size and morphology of the particles was studied. In order to prove successful introduction of Nd^{3+} into the SrF_2 lattice, microstructure and morphology behaviors of the nanoparticles on Nd^{3+} doping were characterized via XRD, FESEM, HRTEM measurements. Additionally to test the sinterability, the obtained $\text{Nd}:\text{SrF}_2$ powder was fabricated to transparent ceramic by vacuum hot press sintering, and the optical transmission spectrum was measured.

2. Experimental section

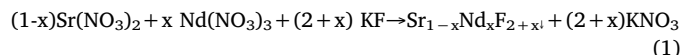
2.1. Chemicals and materials

Nanocrystalline powders of $\text{Sr}_{1-x}\text{Nd}_x\text{F}_{2+x}$ were synthesized using commercially available reagents (produced by Sinopharm Chemical Reagent Co. Ltd, Shanghai, China): hydrated strontium nitrates (99.9%), hydrated neodymium nitrates (99.9%), and hydrated potassium fluoride (99.9%). Water was distilled. There was no further purification of any of the chemicals or reagents used in this study.

2.2. Preparation

One typical sample (1.0 M reactant concentration) was prepared by the following procedures: A solution containing the cationic precursors (Sr^{2+} and Nd^{3+}) was made by dissolving nitrate salts in distilled water. The total concentration of strontium and neodymium ions was 1.0 M with the ration of these two ions determined by the stoichiometric ration of the molecular formula $\text{Sr}_{1-x}\text{Nd}_x\text{F}_{2+x}$. The anion solution (F^-) was made by dissolving KF in distilled water with a concentration of 1.0 M. These two solutions were stirred separately for 5 min. Then the cationic solution was added dropwise to the anion solution which was stirred magnetically. The synthesis can be expressed by the following

chemical equation



Where x is doping level ($x = 0, 2, 5, 8, 15$ and 20 mol%). The mixture aqueous solution was stayed for 4 h at room temperature, and then centrifuged at 11,000 rpm for 15 min. The precipitation obtained from centrifuge tube was washed by ultrasonic dispersing in distilled water 10 min. After repeating 3 times centrifugation, the recovered nanoparticles were oven dried at 80°C for 24 h and crushed in an agate mortar to obtain the final $\text{Sr}_{1-x}\text{Nd}_x\text{F}_{2+x}$ nanopowders.

The obtained powders were filled into a graphite mold with a cavity diameter of 16 mm and sintered in a carbon heated vacuum furnace (Shanghai Chenrong Electrical Furnace Co. Ltd., Shanghai, China), under an axial pressure of 30 MPa and vacuum about 5.0×10^{-3} Pa. The heating rate was $15^\circ\text{C}/\text{min}$, and the annealing time was 120 min.

2.3. Characterization

Powder X-Ray diffraction (XRD) measurements were performed on a D/Max-RB (Rigaku, Japan), using $\text{Cu K}\alpha$ radiation ($\lambda = 1.54056 \text{ \AA}$). The Nd^{3+} content determination of the $\text{Nd}:\text{SrF}_2$ powders were assessed with inductively coupled plasma optical emission spectroscopy (ICP-OES) using Prodigy 7 (Leeman, America) with argon gas pressure of 0.3 MPa. The size and morphology of the products were characterized by field-emission scanning electron microscope (FEMSM; ULTRA, PLUS-43-13, Zeiss, Oberkochen, Germany), equipped with an energy dispersive X-ray spectrometer (EDS), operated at an acceleration voltage of 5 kV. High-resolution transmission electron microscopy (HRTEM) images were obtained from a JEM-2100F (JEOL, Tokyo, Japan) with an accelerating voltage of 200 kV. The optical transmission spectrum pattern of $\text{Nd}:\text{SrF}_2$ transparent ceramic was collected by

Lambda 750 (PerkinElmer, USA). All measurements were performed at room temperature.

3. Results and discussion

3.1. Effects of reactant concentration on particle size and shape

It is well known that reactant concentration plays an important role in size and final morphology of precipitation products. In order to obtain nano-sized SrF₂ particles, four undoped SrF₂ samples with different reactant concentrations (0.1 M, 0.5 M, 1.0 M and 1.5 M) were prepared and FESEM images of these products are shown in Fig. 1a–d, respectively. The product obtained at 0.1 M reactant concentration presents homogenous slab-like morphology with a size of about 400 × 200 × 100 nm. As shown in Fig. 1a, the particles are soft agglomerated and we assume that the grain fragments are generated during the ultrasonic dispersion processes. The morphology in this case is in accord with previously work [28]. With increase in reactant concentration, the particle size decreases dramatically at first to an average size of about 30 nm, with spheroidal morphology at 0.5 M (Fig. 1b), and then mildly decreases to an average size of about 20 nm with amorphous shape at 1.0 M (Fig. 1c). Both 0.5 M and 1.0 M nanoparticles are slightly aggregated. When the reactant concentration raises up to 1.5 M, FESEM image illustrated in Fig. 1d shows a bimodal distribution of the SrF₂ particles, for both large and small crystals are observed. The occurrence of large crystals can be explained as that, 1.5 M reactant concentration offers a large degree of supersaturation to the solution environment and leads to large nucleation rate. In fact, a large number of nucleuses have formed in the fleeting first moment, thus the probability of particle collision is greatly improved. As a result, cone-like grains with a length about 500 nm are finally synthesized. Though both large grains can be obtained at 0.1 M and 1.5 M reactant concentrations, Fig. 1d suggests that the large cone-like grains are formed by oriented close-packing of the small particles, while the slab-like grains obtained at 0.1 M shown in Fig. 1a presents single grain nature with respect. This difference indicates lower crystallinity of the product synthesized at 1.5 M and which has been further demonstrated in XRD patterns. The size evolution as a factor of reactant concentration can be described as:

$$r = \frac{2\sigma\bar{V}}{RT\ln S} \quad (2)$$

where r is critical radius of nucleus, S is the supersaturation level which has a positive correlation with reactant concentration, σ is the interfacial tension, \bar{V} is the molar volume, R is the universal gas constant, T is the absolute temperature. Eq. (2) clearly indicates that with increased supersaturation, the critical radius of nucleus decreases at a given temperature. However, this point cannot be overly stressed because of that the situation will be different at higher reactant concentrations, since smaller nucleus implies larger surface energy and nucleus collision probability which consequently leads to serious agglomeration and increase of grain size. On the other hand, the explanation of morphology changes of the particles observed in present study is suspected to the changes of supersaturation level and driving force for the precipitation [29].

Fig. 2 shows the XRD patterns of these four undoped SrF₂ particles. Broader peaks are presented with increased reactant concentration, revealing lower crystallinity and smaller crystal size. The XRD result is in accord with FESEM measurements.

3.2. Effects of Nd³⁺ doping on microstructure and morphology

The XRD patterns of SrF₂ particles doped with 2–20 mol% Nd³⁺ ions (Sr_{1-x}Nd_xF_{2+x}, $x = 0.02, 0.05, 0.08, 0.15, 0.2$) are shown in Fig. 3a. All the diffraction peaks of the samples can be readily indexed to the pure cubic phase of SrF₂ (space group *Fm3m*) according to the JCPDS file No. 06-0262 without any second phase, indicating SrF₂

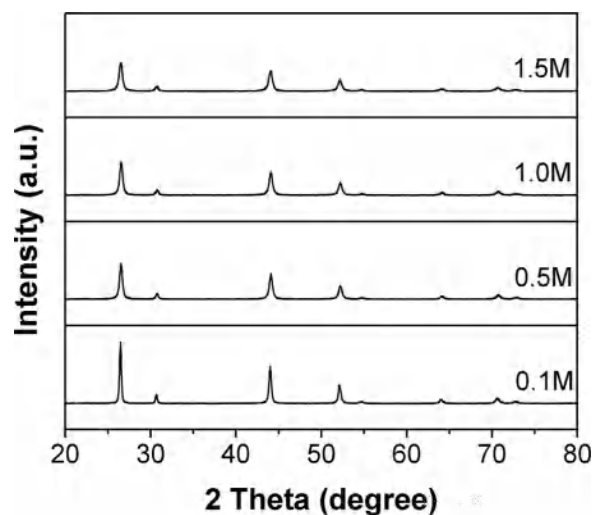


Fig. 2. XRD patterns of the undoped SrF₂ powders.

nanoparticles doped with 2–20 mol% Nd³⁺ ions are isostructural with SrF₂ crystal. This coincides with Yuan et al. [30] and Zhi et al. [31], who reported no second phase was found in 1–20 mol% Nd³⁺ ions and 0.4–40 mol% Er³⁺ ions doped CaF₂, respectively.

From the XRD patterns, the intensities of diffraction peaks are decreased and the full width at half-maximum (FWHM) values are increased with the increase of Nd³⁺ doping, indicating the decrease of crystallinity and crystal size. Notably, it is different with Nd³⁺ doped CaF₂ that, no conspicuous shift of diffraction peak is observed with the increase of Nd³⁺ doping, revealing invariability of Nd:SrF₂ lattice constant. The reason may be that, on one hand, the radius of eight-coordinate Nd³⁺ ions is smaller than Sr²⁺ while close to Ca²⁺ (124.9 pm for Nd³⁺, 140 pm for Sr²⁺, 126 pm for Ca²⁺) [32], the substitution of Nd³⁺ to Sr²⁺ would shrink the lattice constant. On the other hand, charge balance compensating F⁻ ions enter the fluorite structure in interstitial fluoride cubic sites at the same time, and the electronic repulsion between F⁻ ions results in an increase of the lattice parameter. In the case of Nd:SrF₂, the two opposite effects might mostly offset each other. While only the latter effects for Nd:CaF₂, thus resulting in low angle shift in XRD diagram [30].

The average particle sizes and lattice constants of the obtained Nd:SrF₂ nanoparticles were calculated using Scherrer and Bragg equations, respectively. The results are shown in Fig. 3b. The sizes and average values of lattice constants are found to be in ranges of 24–13 nm and 5.805–5.812 Å, respectively. A very slightly expansion trend of the SrF₂ lattice with increase in Nd³⁺ doping presented in Fig. 3b indicates that the electronic repulsion between charge balance compensating F⁻ ions is a little more predominant in the lattice constant evolution with respect to the substitution of Nd³⁺ to Sr²⁺. It should be mentioned that, the regularly shifts of XRD diffraction peaks are used as proofs of successful introduction of impurity ions into the hosts lattice [18,31,33]. However, since the XRD result in present work is not obvious thus not persuasive that the Nd³⁺ ions have been doped into the SrF₂ lattice, it is meaningful to look for other evidence.

Ln³⁺ doping can not only impart new and useful optical properties for many functional nanomaterials, but also be served as an effective way in controlling nanocrystalline size and shape [33,34]. Once the Nd³⁺ ions have entered into the SrF₂ lattice, the final particle morphology and size should have been changed more or less. In order to observe this variation, we prepared Sr_{0.95}Nd_{0.05}F_{2.05} samples at reactant concentrations of 0.1 M and 0.5 M with their FESEM images presented in Fig. 4a, b, respectively. The product obtained at 0.1 M after Nd³⁺ doping shows much smaller size of about 100 nm in length and thinner plate-like morphology compares to that of undoped SrF₂ (Fig. 1a). In the case of 0.5 M, the size and shape of Nd³⁺ doped

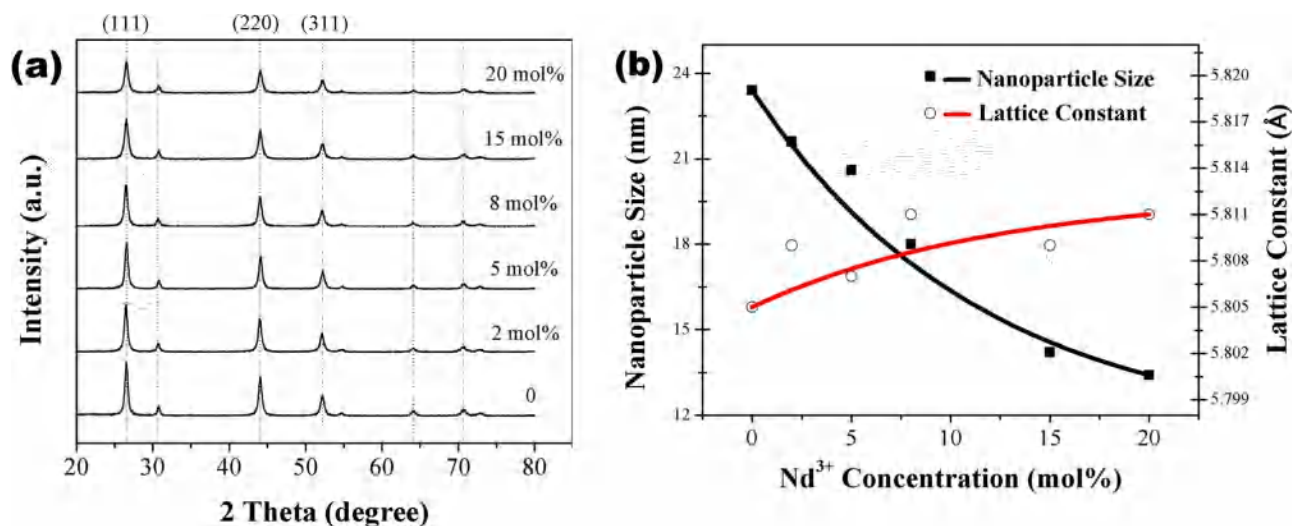


Fig. 3. XRD patterns of SrF₂ nanoparticles with different Nd³⁺ doped concentration (a), and nanoparticle size and lattice constants versus Nd³⁺ concentration (b).

product are similar to the undoped SrF₂ (Fig. 1b). FESEM results indicates that morphology of large size strontium fluoride particles synthesized via precipitation method is more susceptible to Nd³⁺ doping than small size particles. The modifying mechanism had been previously studied by Chen [34], charge compensating F⁻ ions into the grain surface may induce transient electric dipoles with their negative poles outward, and these transient electric dipoles hinder the diffusion of F⁻ ions from the solution to the grain surface, thus retarding the growth of the SrF₂ grains. However, when the crystalline size is very small, the surface energy is large enough to dominate grain growth. Additionally, the explosive nucleation and growing rates, which are drawbacks of precipitation synthesis, finally lead to irregularly shape and fairly aggregated dispersity.

To find more evidences proving Nd³⁺ ions has been effectively doped into the SrF₂ lattice, further insight into the microstructure evolution of SrF₂ after Nd³⁺ doping was afforded by HRTEM. Images displayed in Fig. 5a, c corresponds to the nanoparticles of undoped and Nd³⁺ doped SrF₂ at 0.5 M reactant concentration, respectively. The FFT images are taken as inset. Magnified pictures of selected areas are presented in Fig. 5b, d for a better observation. The pure SrF₂ crystal is well crystalline according to Fig. 5b for its well-laid-out and highly ordered lattice fringe. The observed characteristic space is 0.329 nm, which matches the (111) lattice plane of strontium fluoride. The Nd³⁺ doped SrF₂ sample (Fig. 5d) shows un-continuous and disordered lattice fringe compares to that of undoped SrF₂, indicating the formation of lattice defects which originated ascribe to the introduction of Nd³⁺ ions

into the SrF₂ lattice. The lattice fringe distances were measured to 0.331, 0.291 and 0.206 nm in this case, which are associated with the (111), (200) and (220) interplanar space of SrF₂. Although obvious lattice distortion is observed in the HRTEM image when doped with Nd³⁺, it is not contrary to XRD result that no evident regular shift is presented, since XRD reflects the macroscopic nature of the whole sample while HRTEM takes the microscopic pictures in a small local place which clearly recorded the influence of the two opposite effects (discussed above) on lattice evolution. Therefore, HRTEM images shows poorer crystalline and lower structural uniformity of SrF₂ nanocrystal after Nd³⁺ doping, thus suggesting successful introduction of Nd³⁺ ions into the SrF₂ lattice.

Furthermore, the actual doping contents of Nd³⁺ ions in the Sr_{1-x}Nd_xF_{2+x} (x = 0.02, 0.05, 0.08, 0.15 and 0.2) powder products are quantitatively determined by ICP-OES analysis and the results with respect to designed contents of the starting reagents are listed in Table 1. The actual Nd³⁺ contents are 1.88 mol% for the x = 0.02 sample, 4.36 mol% for the x = 0.05 sample, 7.23 mol% for the x = 8 sample, 14.17 mol% for the x = 0.15 sample and 19.14 mol% for the x = 0.2 sample. This as well confirms a good incorporation of the Nd³⁺ ions in the SrF₂ products, for only a very small amount of Nd³⁺ loss in the final powder products compared with the starting solutions.

3.3. Sintering of the synthesized powder

The synthesized nanopowder doped with 5 mol% Nd³⁺ was

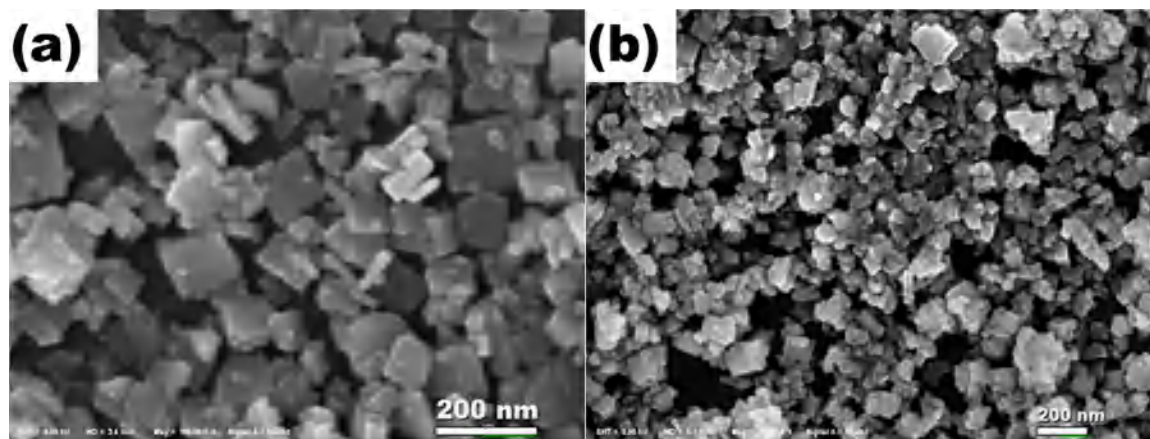


Fig. 4. FESEM images of Sr_{0.95}Nd_{0.05}F_{2.05} nanopowders with different reactant concentration. (a) 0.1 M; (b) 0.5 M.

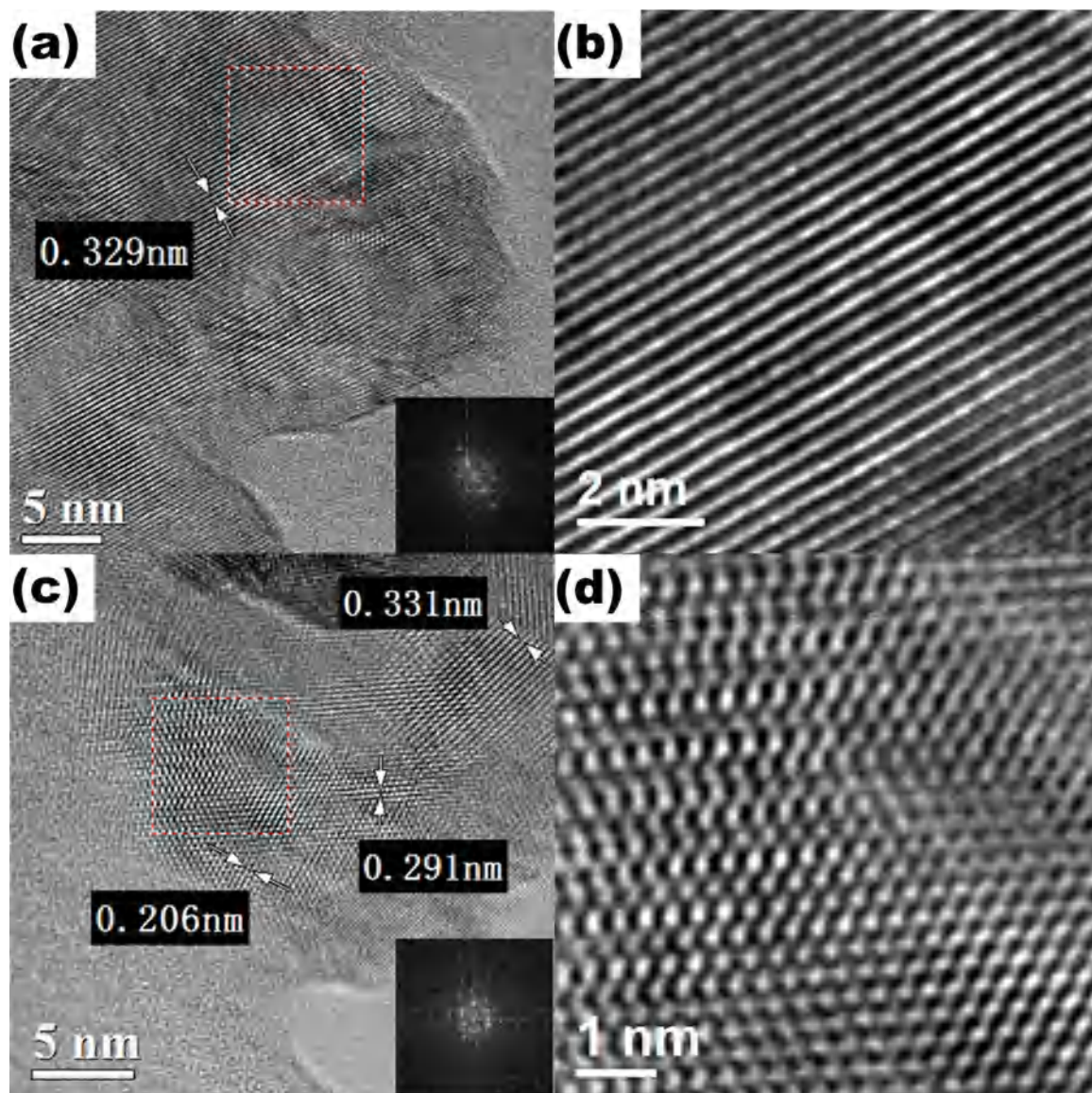


Fig. 5. HRTEM graphs of (a) SrF_2 and (c) Nd^{3+} doped SrF_2 , FFT images are taken as inset. (b) and (d) are the magnified pictures of selected areas of SrF_2 and Nd^{3+} doped SrF_2 , respectively.

Table 1
Comparison of designed contents with ICP results of the samples.

Samples	Nd^{3+} content (mol%)				
Starting reagents (designed contents)	2	5	8	15	20
Powder products (ICP results)	1.88	4.36	7.23	14.17	19.14

sintered at 800 °C for 120 min in a vacuum environment under 30 MPa pressure to test the sinterability. Inset of Fig. 6a shows the appearance of $\text{Nd}:\text{SrF}_2$ transparent ceramic sample with a diameter of 16 mm and a thickness of 2 mm. It can be seen that the ceramic is transparently by naked eye and the letters can be recognized distinctly. Fig. 6b presents FESEM micrograph of the sintered sample and almost no pore is observed in the fracture surfaces. The fracture modes are mainly intergranular. Grain size of the 5 mol% Nd^{3+} doped SrF_2 transparent ceramic sample is in range of about 0.5–1 μm , and the grain boundary is clean without any trace of secondary phases. EDS spectrum of the ceramic section (inset of Fig. 6b) verified the effectively incorporation of Nd^{3+} ions into the SrF_2 nanocrystals, as the actual content of Nd^{3+} was measured to 4.66 mol%. This value is slightly higher than the

actual content of Nd^{3+} ions in $\text{Sr}_{0.95}\text{Nd}_{0.05}\text{F}_{2.05}$ powder product, as due to the loss in the amount of absorbed water (or hydroxyl groups) and nitrates during the sintering process [31]. Fig. 6a shows optical transmission spectrum of the sample, as can be seen, the optical transmission of the 5 mol% Nd^{3+} doped SrF_2 transparent ceramic at 1060 nm is about 80%. Low optical transmission in the ~ 500 nm range indicates the existence of embedded pores. As reported by Xu and co-workers [35], the generation of these residual pores is attributed to the irregularly shape and unevenly size distribution of the precursor powder. Generally, the residual pores as well as the secondary phases are the main scattering factors, and will do harm to the transmission of transparent ceramics. Thus, it is important to eliminate these small pores, in order to obtain ceramics with high optical properties and realize high-power laser output.

4. Conclusion

The undoped and Nd^{3+} doped strontium fluoride nanoparticles were synthesized by a chemical precipitation method, using hydrated strontium fluoride, hydrated neodymium nitrates and hydrated potassium fluoride as starting materials. It is found that the reactant

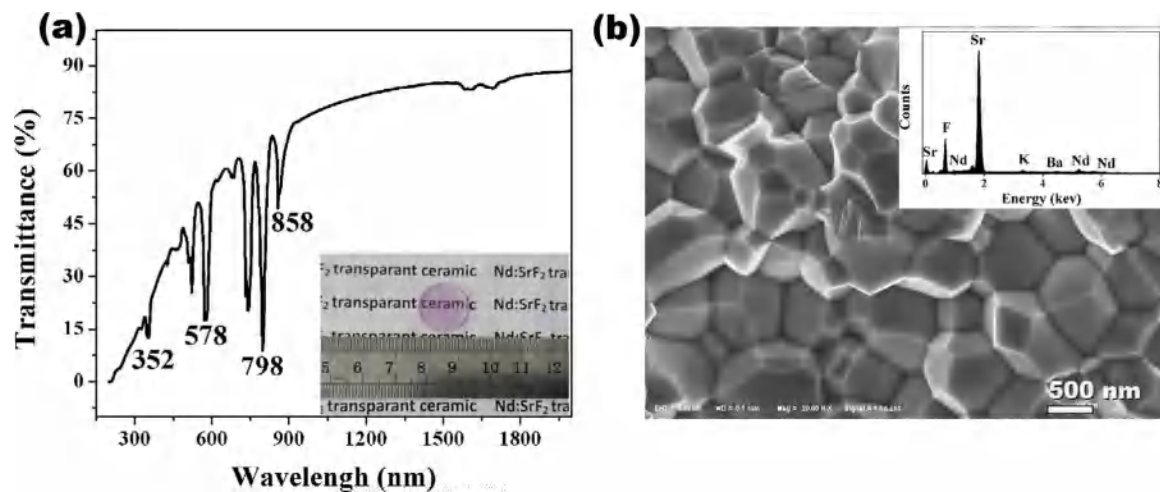


Fig. 6. (a) Optical transmission and (b) FESEM micrograph of the 5 mol% Nd^{3+} doped SrF_2 transparent ceramic sintered at 800°C for 2 h. Insets in (a), (b) are the appearance and the EDS spectrum of the ceramic, respectively.

concentration has played an important role in morphology and size of the powders. When the molar concentration of starting materials increases from 0.1M to 1.5 M, the morphology of undoped SrF_2 grains evaluate from slab-like shape with $400 \times 200 \times 100$ nm in size to irregularly or near sphere shape with 15–30 nm in size, then the small particles seriously aggregate to cone-like grain with mean size of 500 nm. The obtained SrF_2 nanoparticles with Nd^{3+} doping concentration up to 20 mol% keep a single cubic fluoride structure. With the increase of Nd^{3+} doping, the grain size and crystallinity decreased. However, the lattice constant lacks sensitivity to Nd^{3+} doping as a consequence of two opposite effects: the formation of interstitial fluorine ions expands the SrF_2 lattice while the substitution of Nd^{3+} to Sr^{2+} shrinks it. The observed disordered lattice fringe suggests successful introduction of Nd^{3+} ions into the SrF_2 lattice.

The synthesized powders have good sinterability and can be fabricated to transparent ceramics with a transmittance of about 80% at 1060 nm by vacuum hot pressed sintering at 800°C for 2 h.

Acknowledgment

This work was financially supported by the National Natural Science Foundation of China (No. 51432007).

References

- [1] E. Downing, L. Hesselink, J. Ralston, R. Macfarlane, A three-color, solid state, three-dimensional display, *Science* 273 (1996) 1185–1189.
- [2] L.B. Su, Q.G. Wang, H.J. Li, G. Brasse, P. Gamy, J.L. Doualan, A. Braud, R. Moncorge, Y.Y. Zheng, X.B. Qian, J. Xu, Spectroscopic properties and CW laser operation of Nd, Y-codoped CaF_2 single crystals, *Laser Phys. Lett.* 10 (2013) 390–392.
- [3] G.S. Yi, H.C. Lu, S.Y. Zhao, Y. Ge, W.J. Yang, D.P. Chen, H.L. Guo, Synthesis, characterization, and biological application of size-controlled nanocrystalline $\text{NaYF}_4:\text{Yb,Er}$ infrared-to-visible up-conversion phosphors, *Nano Lett.* 4 (2004) 2191–2196.
- [4] Y.B. Mao, F. Zhang, S.S. Wong, Ambient template-directed synthesis of single-crystalline alkaline-earth metal fluoride nanowires, *Adv. Mater.* 18 (2006) 1895–1899.
- [5] V.V. Osipov, V.A. Shitov, V.I. Solomonov, K.E. Lukyashin, A.V. Spirina, R.N. Maksimov, Composite $\text{Nd:YAG/Cr}^{4+}:\text{YAG}$ transparent ceramics for thin disk lasers, *Ceram. Int.* 41 (2015) 13277–13280.
- [6] A.P. Alivisatos, Semiconductor clusters, nanocrystals and quantum dots, *Science* 271 (1996) 993.
- [7] Y.N. Xia, P.D. Yang, Y.G. Sun, Y.Y. Wu, B. Mayers, Y.B. Gates, D. Yin, F. Kim, Y.Q. Yan, One-dimensional nanostructures: synthesis, characterization, and applications, *Adv. Mater.* 15 (2003) 353–389.
- [8] C. Burda, X. Chen, R. Narayanan, M.A. El-sayed, Chemistry and properties of nanocrystals of different shapes, *Chem. Rev.* 105 (2005) 1025–1102.
- [9] S. Li, T. Xie, Q. Peng, Y.D. Li, Nucleation and growth of CeF_3 and NaCeF_4 nanocrystals, *Chem. Eur. J.* 15 (2009) 2512–2517.
- [10] F. Estebanbetegon, C. Zaldo, C. Cascales, Hydrothermal Yb^{3+} -doped $\text{NaGd}(\text{WO}_4)_2$ nano- and micrometer-sized crystals with preserved photoluminescence properties, *Chem. Mater.* 22 (2010) 2315–2324.
- [11] K. Thoralf, S. Cudrum, K. Erhard, Solid solutions $\text{CaF}_2\text{--YF}_3$ with fluorite structure prepared on the sol–gel route: investigation by multinuclear MAS NMR spectroscopy, *J. Phys. Chem. C* 118 (2014) 21066–21074.
- [12] Y.Y. Li, J.P. Liu, X.T. Huang, G.Y. Li, Hydrothermal synthesis of Bi_2WO_6 uniform hierarchical microspheres, *Cryst. Growth Des.* 7 (2007) 1350–1355.
- [13] J.Y. Lao, J.G. Wen, Z.F. Ren, Hierarchical ZnO nanostructures, *Nano Lett.* 2 (2002) 1287–1291.
- [14] J. Li, F. Chen, W.B. Liu, W.X. Zhang, L. Wang, X.W. Ba, Y.J. Zhu, Y.B. Pan, J.K. Guo, Co-precipitation synthesis route to yttrium aluminum garnet (YAG) transparent ceramics, *J. Eur. Ceram. Soc.* 32 (2012) 2971–2979.
- [15] Z.D. Liu, B.C. Mei, J.H. Song, W.W. Li, Optical characterizations of hot-pressed erbium-doped calcium fluoride transparent ceramic, *J. Am. Ceram. Soc.* 97 (2014) 2506–2510.
- [16] H.M. Qin, X.J. Tan, W.C. Huang, J. Jiang, H.C. Jiang, Application of urea precipitation method in preparation of advanced ceramic powders, *Ceram. Int.* 41 (2015) 11598–11604.
- [17] J.G. Li, X.D. Li, X.D. Sun, T. Ikegami, T. Ishigaki, Uniform colloidal spheres for $(\text{Y}_{1-x}\text{Gd}_x)_2\text{O}_3$ ($x = 0\text{--}1$): formation mechanism, compositional impacts, and physico-chemical properties of the oxides, *Chem. Mater.* 6 (2008) 2274–2281.
- [18] S.Y. Yao, X. Zhou, Y.L. Huang, Z.S. Wang, Y.M. Long, W.F. Li, Luminescent properties of Bi^{3+} -activated $\text{Ca}_2\text{Sb}_2\text{O}_7$ nano-phosphor prepared by co-precipitation method, *J. Alloy. Compd.* 653 (2015) 345–350.
- [19] A.D. Rubloff, Equilibria among point defects in GdF_3 -doped CaF_2 , *J. Chem. Phys.* 64 (1976) 1509–1515.
- [20] G.W. Rubloff, Far-ultraviolet reflectance spectra and the electronic structure of ionic crystals, *Phys. Rev. B* 5 (1972) 662–684.
- [21] R. Srivastava, H.V.L. Jr, L.L. Chase, W.E. Bron, Raman frequencies of fluorite crystals, *Phys. Lett.* 36A (1971) 333–334.
- [22] O.K. Alimov, T.T. Basiev, M.E. Doroshenko, P.P. Fedorov, V.A. Konyushkin, A.N. Nakladov, V.V. Osiko, Investigation of Nd^{3+} ions spectroscopic and laser properties in SrF_2 fluoride single crystal, *Opt. Mater.* 34 (2012) 799–802.
- [23] W.W. Li, B.C. Mei, J.H. Song, Nd^{3+} , Y^{3+} -codoped SrF_2 laser ceramics, *Opt. Mater.* 47 (2015) 108–111.
- [24] S.A. Payne, J.A. Caird, L.L. Chase, L.K. Smith, N.D. Nielsen, W.F. Krupke, Spectroscopy and laser properties of Nd^{3+} -Doped CaF_2 , SrF_2 , and BaF_2 , *Adv. Solid State Lasers* (1990).
- [25] X.Y. Liu, B.C. Mei, W.W. Li, Z.C. Sun, Z.D. Liu, L.B. Su, Effect of sintering temperature on the microstructure and transparency of Nd, Y:CaF₂ ceramics, *Ceram. Int.* 42 (2016) 13285–13290.
- [26] W.W. Li, Z.D. Liu, Z.W. Zhou, J.H. Song, B.C. Mei, L.B. Su, Characterizations of a hot-pressed Er and Y codoped CaF_2 transparent ceramic, *J. Eur. Ceram. Soc.* 36 (2016) 3481–3486.
- [27] W.W. Li, H.J. Huang, B.C. Mei, J.H. Song, Comparison of commercial and synthesized CaF_2 powders for preparing transparent ceramics, *Ceram. Int.* 43 (2017) 10403–10409.
- [28] A.A. Luginina, P.P. Fedorov, S.V. Kuznetsov, M.N. Mayakova, V.V. Osiko, V.K. Ivanov, A.E. Baranchikov, Synthesis of ultrafine fluorite $\text{Sr}_{1-x}\text{Nd}_x\text{F}_2+x$ powders, *Inorg. Mater.* 48 (2012) 531–538.
- [29] R. Kumar, K.H. Prakash, P. Cheang, A.K. Khor, Temperature driven morphological changes of chemically precipitation hydroxyapatite nanoparticles, *Langmuir* 20 (2004) 5196–5200.
- [30] D. Yuan, W.W. Li, B.C. Mei, J.H. Song, Synthesis and characterization of Nd^{3+} -Doped CaF_2 nanoparticles, *J. Nanosci. Nanotechnol.* 15 (2015) 9741–9745.
- [31] G.L. Zhi, J.H. Song, B.C. Mei, W.B. Zhou, Synthesis and characterization of Er^{3+} -Doped CaF_2 nanoparticles, *J. Alloy. Compd.* 509 (2011) 9133–9137.
- [32] R.D. Shannon, Revised effective ionic radii and systematic studies of interatomic distances in halides and chalcogenides, *Acta Crystallogr. A* 32 (1976) 751–767.

- [33] F. Wang, Y. Han, C.S. Lim, Y.H. Lu, J. Wang, J. Xu, H.Y. Chen, C. Zhang, M.H. Hong, X.G. Liu, Simultaneous phase and size control of upconversion nanocrystals through lanthanide doping, *Nature* 463 (2010) 1061–1065.
- [34] D.Q. Chen, Y.L. Yu, F. Huang, P. Huang, A.P. Yang, Y.S. Wang, Modifying the size and shape of monodisperse bifunctional alkaline-earth fluoride nanocrystals through lanthanide doping, *J. Am. Chem. Soc.* 132 (2010) 9976–9978.
- [35] X.J. Xu, X.D. Sun, H. Liu, J.G. Li, X.D. Li, D. Huo, S.H. Liu, Synthesis of monodispersed spherical yttrium aluminum garnet (YAG) powders by a homogeneous precipitation method, *J. Am. Ceram. Soc.* 95 (2012) 3821–3826.